Int. J. Electrochem. Sci., 7 **(2012)** 7140 - 7151

International Journal of
ELECTROCHEMICAL
SCIENCE
www.electrochemsci.org

Pd and Pd-Co Oxygen Reduction Nanocatalysts in Acidic Media

Adarely Velasco Martínez[1], *Miguel Torres Rodríguez*[1,*], *Mirella Gutiérrez Arzaluz*[1], *Paz del Ángel Vicente*[2], *Omar Solorza Feria*[3].

[1] Área de Química Aplicada, Universidad Autónoma Metropolitana, Azcapotzalco, Av. San Pablo 180, Col. Reynosa. C.P. 02200, México, D.F.
[2] Instituto Mexicano del Petróleo, eje Central Lázaro Cárdenas 152, C.P. 07730, México, D.F.
[3] Depto. de Química, Cinvestav-IPN.. Av. Instituto Politécnico Nacional, 2508, Col. San Pedro Zacatenco. C.P. 07360, México, D.F.
[*]E-mail: trm@correo.azc.uam.mx

Received: 1 June 2012 / *Accepted:* 28 June 2012 / *Published:* 1 August 2012

Palladium (Pd) and palladium-cobalt (Pd-Co) nanocatalysts were successfully synthesized by the chemical reduction method and characterized for the molecular oxygen reduction reaction (ORR) in acid medium. Both Pd and Pd-Co nanoparticles were prepared by the chemical reduction of palladium (II) chloride, $PdCl_2$, and cobalt (II) chloride, $CoCl_2$, as precursors and polyvinylpyrrolidine (PVP) as a protecting agent. The synthesized Pd/C and Pd-Co/C materials were characterized by X-ray diffraction (XRD) and transmission electron microscopy (TEM). Results conducted to the formation of bimetallic nanoparticles with an average size of 5 to 12 nm and a good dispersion of Pd-Co on carbon, as well as the formation of some nano-sized clusters particles. The crystallographic planes identified as (111) and a (200) corresponds to the formation of face-centered cubic (FCC) Pd with nanocrystalline structure.The nanocatalyst were supported on Vulcan® carbon XC-72 by the impregnation method and their electrochemical activity for the ORR was evaluated by cyclic voltammetry and rotating disk electrode techniques. The obtained results demonstrated that the Pd-based catalysts promoted the activity toward the ORR through a multi-electron charge transfer mechanism for the oxygen reduction to water formation.

Keywords: nanoparticles, Pd, Pd-Co, electrocatalysts, oxygen reduction reaction (ORR).

1. INTRODUCTION

At present, most of the energy generated in the world comes from the combustion of fossil fuels. The constant fluctuation of oil prices and the environmental consequences generated by the combustion of fossil fuels have led to the greater awareness of the effects of fossil fuels on climate change. As a result, policies have been developed that seek to boost the clean energy sector by

developing advanced technologies to promote environmentally respectable and sustainable development.

The proton exchange membrane (PEM) fuel cells represent a source of efficient and sustainable technology for the generation of energy, but there are several limitations inherent in the sluggish kinetics of the oxygen reduction reaction (ORR). For example, this reaction is at least three orders of magnitude slower than the hydrogen oxidation reaction (HOR). Therefore, it is necessary to develop novel catalysts and a new route of synthesis for the cathode electrocatalysts to improve their activity, selectivity and stability. The typical materials used in PEM fuel cells are based on platinum and its alloys [1,3]; however, the use of Pt presents several limitations: a high cost for use in fuel cells and high sensitive to the presence of CO, which, when adsorbed on the surface, causes a decrease in efficiency. Therefore, we have investigated a new composition of catalysts that selectively catalyze the ORR for use in the PEM fuel cells. We are investigating alloys based on Pd nanoparticles as the electrocatalyst for the ORR because Pd is more abundant and less expensive relative to Pt (www.kitco.com/charts/livepalladium), it presents considerable catalytic activity for the ORR in an acidic electrolyte, which should preferably take place through track four electrons [4-14]. Wang and Balbuena [7] reported an induced change in the ORR for the Gibbs free energy for Pd-Co bimetallic electrocatalysts, resulting in an increase in the kinetics of the ORR. Fernandez et al [15] assume the increased activity of an alloy occurred via a thermodynamic model, reporting the ease of dissociation of the O_2 by the incorporation of active metals such as Co to Pd-based catalysts. Zhang and a colleague [9-10], Wang and colleagues [16] and Li and colleagues [17] have reported that the effect of the catalytic activity towards ORR varies depending on particle size, morphology and density, derived from the synthesis method employed and the ratio of Pd to Co used. Hence, this work is focused on synthesizing nanoparticles of Pd and Pd-Co as nanocatalysts for the ORR, in order to improve the kinetic properties of the single Pd metal nanoparticles through a synergistic effect via the incorporation of a second metal. The result show a good control on the composition and atomic structure of these nanoparticles which are then assessed for their electrocatalytic activity as the cathode electrode in PEM fuel cells.

2. EXPERIMENTAL

2.1 Electrocatalysts preparation

In the first stage monometallic particles were synthesized in solution, according to an experimental method reported in the literature [18-21] with some modifications. Briefly, a H_2PdCl_4 solution was prepared by the addition of 0.2083 g of $PdCl_2$ ($1.174 \cdot 10^{-3}$ mol) and 1.5 mL of 0.2 mol L^{-1} HCl, then this solution was added to a solution containing 2.59 g of polyvinylpyrrolidone (PVP) (23.84 mol L^{-1}, Mw = 55,000), (molar ratio PVP:Pd= 20) and 50 ml of deionized H_2O. Thereafter, a solution of 0.5 M NH_4OH (pH=8) was added drop-wise to the above solution, and immediately afterwards, a mixture of H_2O/C_2H_5OH (5/15 ml) was added in order to carry out the reduction of Pd^{+2}. The reaction mixture was heated at a temperature to reflux (80 °C) for 3 h, with continuous stirring to obtain a

homogenous colloidal dispersion of intense brown coloration. In a second step, bimetallic nanoparticles Pd-Co were synthesized according to the reported "co-reduction method" [20, 22]. To the synthesized colloidal Pd nanoparticles, a 0.0169 g solution of $CoCl_2.6H_2O$ ($7.1 \cdot 10^{-6}$ mol L^{-1}) was added slowly, as a precursor of the cobalt species, following the same methodology described above..

Supported nanoparticles were prepared by the addition of a solution containing monometallic Pd or bimetallic Pd-Co nanoparticles in a solution over 0.375 g of Vulcan® XC-72, maintaining a vigorous stirring for 1 h. The solvent was removed by heating, and the precipitated powder was thermally treated at 450 °C with a flow of air-N_2 and H_2 to activate the nanoparticles. Both Pd and Pd-Co catalysts were classified according to the metal loading and the heat treatment as shown in Table 1, which summarizes the prepared samples, as well as the nomenclature.

Table 1. Pd and Pd-Co catalysts loading assignations

Electrocatalysts	M/C (wt %)	Treatment conditions	Sample
Pd	Solution		Pd sol
	Metallic	N_2/H_2-Air	Pdm
	5 %		(Pd/C5)1
	10 %		(Pd/C10)1
	25 %	without treatment	Pd/C25(w/t)
		$N2/H_2$-Air	(Pd/C25)1a
		N_2/H_2	(Pd/C25)2b
Pd-Co		without treatment	Pd-Co/C25(w/t)
		N_2/H_2-Air	(Pd-Co/C25)1a
		N_2/H_2	(Pd-Co/C25)2b
		N_2/H_2-Air	(Pd-Co/C25)3c

[a] Sample $(M/C_{25})_1$ corresponds to a catalyst that was subjected to the following heat treatments: calcinations at 450 °C for 30 min in an air-N_2 (50-50 %v) mixture, followed by a step of H_2 for 2 h.
[b] The samples $(M/C_{25})_2$ correspond to catalysts that were subjected to calcinations: 450 °C for 30 min in an atmosphere of N_2 followed by a step of H_2 for 2 h.

2.2 Physical characterization

The formation of Pd nanoparticles was monitored by UV-Vis spectroscopy (Shimadzu UV-1800). An X-ray diffractometer (XRD Siemens D-500 with Cu tube at 35kV and 25 mA) and monochromator to remove K_β radiation were used to determine the crystal structure of the nanoparticles synthesized in range from 3 to 90° (2θ) with a run rate of 0.04°/s. The samples were studied by a high-resolution transmission electron microscopy (HRTEM); the micrographs were obtained in a TITAN 80-300 with a Schottky-type field emission gun operating at 300 kV. The point resolution and the information limit were better than 0.085 nm. The HRTEM digital images were obtained using a CCD camera and digital micrograph software from GATAN. High angle annular dark

field image (HAADF) was obtained in a scanning and transmission electron microscope (STEM) (JEOL JEM-2200FS) with a Schottky-type field emission gun operating at 200 kV. The HAADF technique can resolve interfaces/ locations between different elements since the image intensity from an element (atomic number Z) follows approximately a Z^2 dependence. The elemental composition and mapping were obtained by Energy dispersive X-ray spectroscopy (EDS) with a NORAN spectrometer fitted to the STEM. The powder samples were ultrasonically dispersed in ethanol and supported on holey carbon coated copper grids to prepare the materials for observation.

2.3 Electrode preparation for the electrochemical study

Electrochemical techniques of cyclic voltammetry (CV) and rotating disk electrode (RDE) were performed in a potentiostat-galvanostat (EG&G, PARC model 2273) with PARSTAT® software for data adquisition and control of the rotation rate of the RDE.

The ORR was evaluated at room temperature in a typical three electrochemical cell, consisting of a working electrode (glassy carbon disk, 3 mm in diameter, with a geometric area of 0.0706 cm^2), a counter electrode (Platinum mesh) and a saturated mercuric sulfate reference electrode ($Hg/Hg_2SO_{4(sat)}/H_2SO_4$ 0.5M) with 0.68V vs. NHE. FreshH_2SO_4 0.5 M solution was used as electrolyte. Some drops of solution, previously prepared by mixing 50 μL of 2-propanol, 5 μL Nafion (5%) and 2 mg of electrocatalyst, was deposited onto the surface of the glassy carbon electrode to form a thin film working electrode. The working electrode surface activation were carried out in a N_2-saturated H_2SO_4 solution attained by bubbling N_2 into the solution for 20 minthen sweeping the electrode potential from 0 to 1.6V (NHE) at a scan rate of 100 mV/s. Thereafter, at the end of the activation process, the electrolyte was saturated with pure O_2 for 20 min, until a steady state open circuit potential was reached. The RDE measurements were performed on different rotational speeds from 100 to 2500 rpm, with a scan rate of 5 mV/s.

3. RESULTS AND DISCUSSION

The reduction of Pd^{2+} to Pd^0 nanoparticles was monitored by UV-Vis spectroscopy in the range of 220-600 nm. Figure 1 shows the absorption spectra of solutions at different times of reduction, the absorption bands for the reference sample (Pd solution), are attributed to the absorption of the Pd^{2+} species, the solution before the reduction presents a pale yellow color, showing a peak at 330 nm in the spectrum, this is due to a charge transfer transition of the $[PdCl_4]^{-2}$ ions [18, 23]. During the reduction reaction, the decline and consecutive disappearance of the absorption peak is notorious, attributed to the Pd^{2+} ions reduction which are completely reduced after 15 minutes; furthermore, an increase in the absorbance of the solution due to the change in the color intensity was observed.

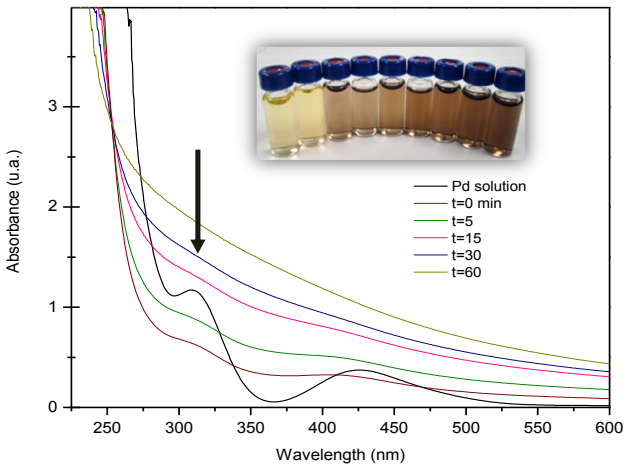

Figure 1. UV-Visible spectra during the formation of Pd nanoparticles.

The XRD patterns corresponding to the Pd/C monometallic and Pd-Co/C bimetallic catalysts with different composition of Pd on carbon were subjected to different heat treatments which results are shown in Figure 2. The Pd characteristic peaks appears at angles of 2θ = 40, 47, 67 and 82 degrees corresponding to the crystallographic orientation planes of (111), (200), (220) and (311), respectively (JCPDS-87-0641). The first peak at 2θ 25 degrees is attributed to a carbon-type hexagonal structure (002) plane, Vulcan XC-72 used as catalysts support.

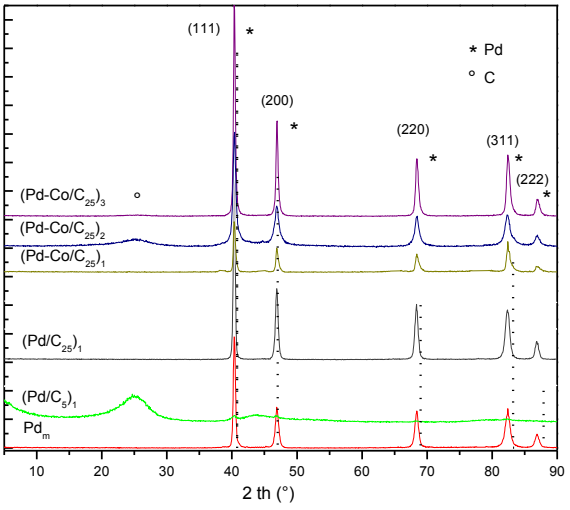

Figure 2. XRD patterns of Pd and Pd-Co catalysts with different metal loadings.

Figure 3 presents several high-resolution images (HRTEM) of the $(Pd/C_5)_1$ catalyst, featuring narrow size distribution of particle size in the range from (3-10 nm); in the same micrographs,

laminar planes can be observed, which is characteristic of the support (Vulcan carbon XC-72). Thus, Fast Fourier transforms (FFT) were also performed from the high resolution images which show (111) and (200) crystallographic planes characteristic of hexagonal fcc phase of Pd.

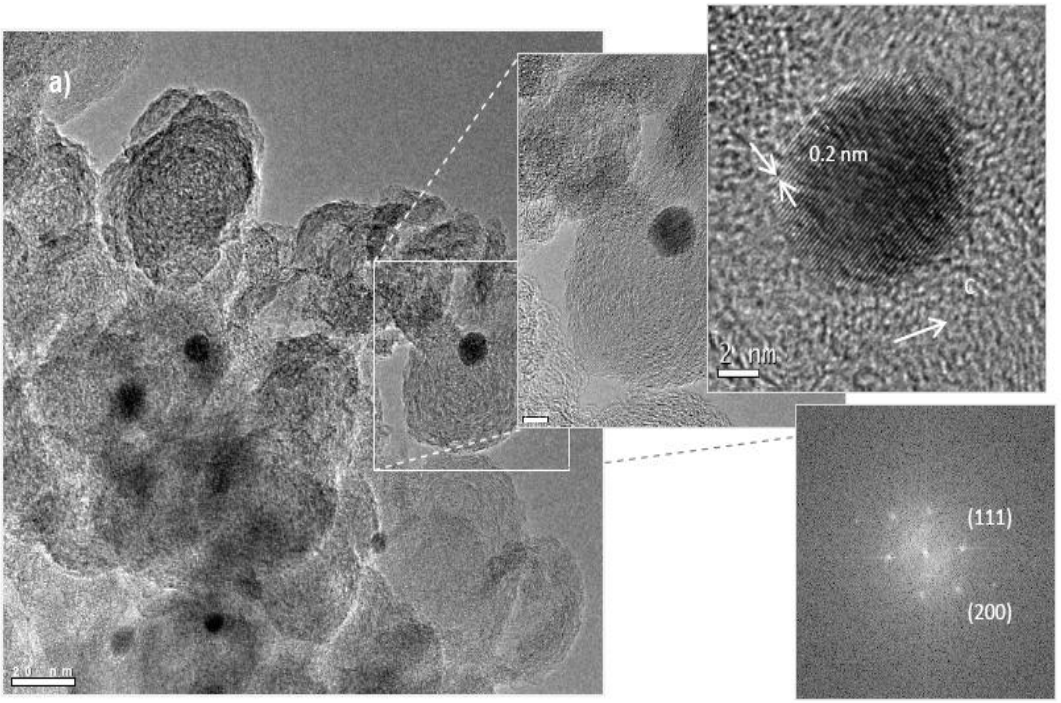

Figure 3. High-resolution images of the $(Pd/C_5)_1$ catalyst. The nanoparticle was indexed like Pd by using FFT.

The results of the TEM analysis of the $(Pd\text{-}Co/C_{25})_3$ catalyst are shown in Figure 4; the particle size distribution of Pd-Co is in the range from 3-15 nm with a spherical morphology. Chemical composition from EDX analysis confirms the presence of both metals (Pd and Co). This is corroborated by the use of the HAADF-STEM and EDX-STEM techniques as depicted in Figures 4 and 5. The Z-contrast images in figure 5 show bright Co (Z=27) and relatively darker Pd (Z=46), which suggest the formation of a nanoalloy structure [24]. These results show a random mixed Pd-Co nanoalloys, which suggests that this compound is formed; the largest content of metals correspond to Pd as shown in various regions where a mapping were performed.

Elemental Chemical EDX analysis was performed to confirm the presence of palladium as monometallic catalysts, and palladium and cobalt as bimetallic catalysts in the samples. In the bimetallic sample, palladium was observed to have the highest intensity of the peaks, in agreement with the synthesis of the Pd-Co nanoalloys . These results confirm a good incorporation of Co into Pd, obtaining dispersion at the atomic level. The results of the HAASF-STEM and a molar ratio of Pd:Co = 3 for the precursor solutions suggest the formation of a stable electrocatalyst alloy.

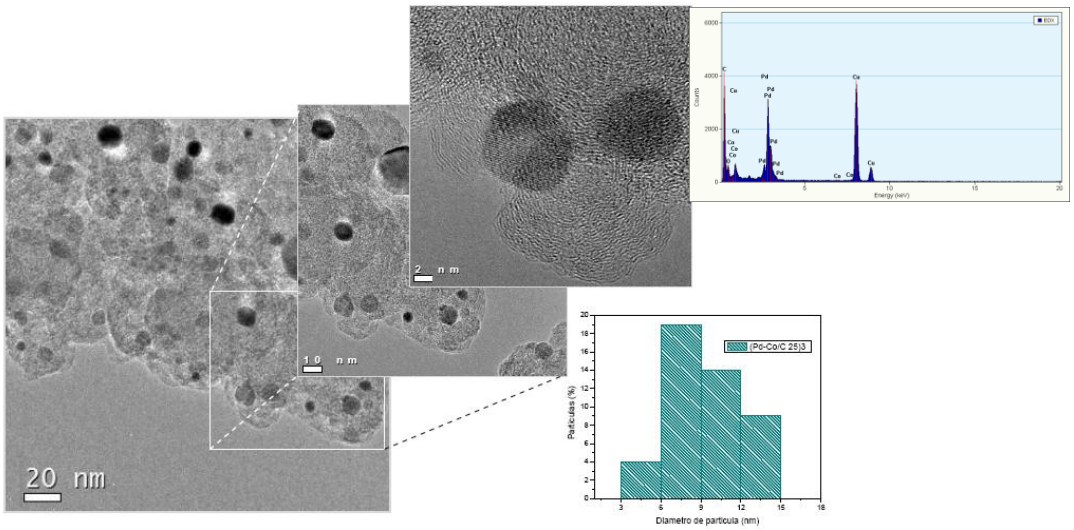

Figure 4. HRTEM image and EDX of $(Pd\text{-}Co/C_{25})_3$ catalyst and its corresponding particle size distribution.

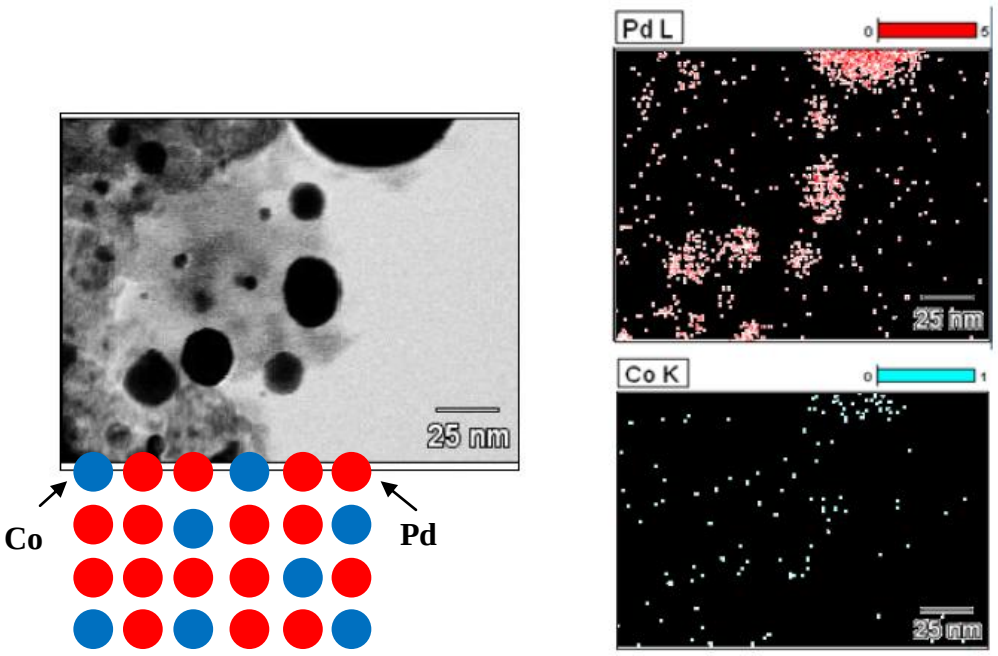

Figure 5. Images of HAADF-STEM and mapping of the $(Pd\text{-}Co/C_{25})_3$ bimetallic catalyst.

It is well known that the ORR kinetics strongly depends on the crystallographic orientation of the particles composed electrodes and on the electrolyte used in the experiments. Figure 6 shows cyclic voltammograms of Pd_m, $(Pd/C_{25})_1$, $(Pd\text{-}Co/C_{25})_1$ and $(Pd\text{-}Co/C_{25})_3$ in N_2-saturated 0.5 M H_2SO_4, distinguishing the increase of the current density in the anodic side on both PdCo catalysts when compared to Pd alone. The voltammogram responses are influenced by the particle size of the supported bimetallic compounds.

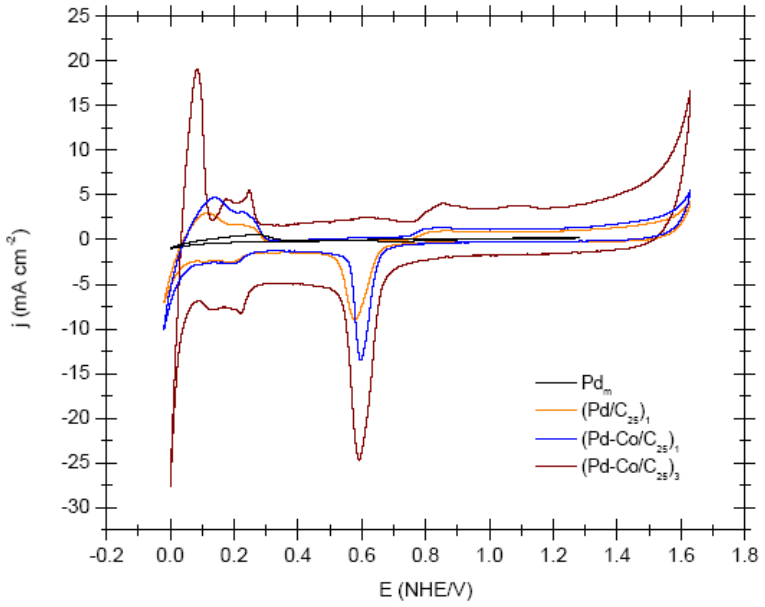

Figure 6. Cyclic voltammograms of Pd and PdCo/C electrodes in N_2-saturated 0.5 M H_2SO_4. Scan rate is 100 mV s^{-1}.

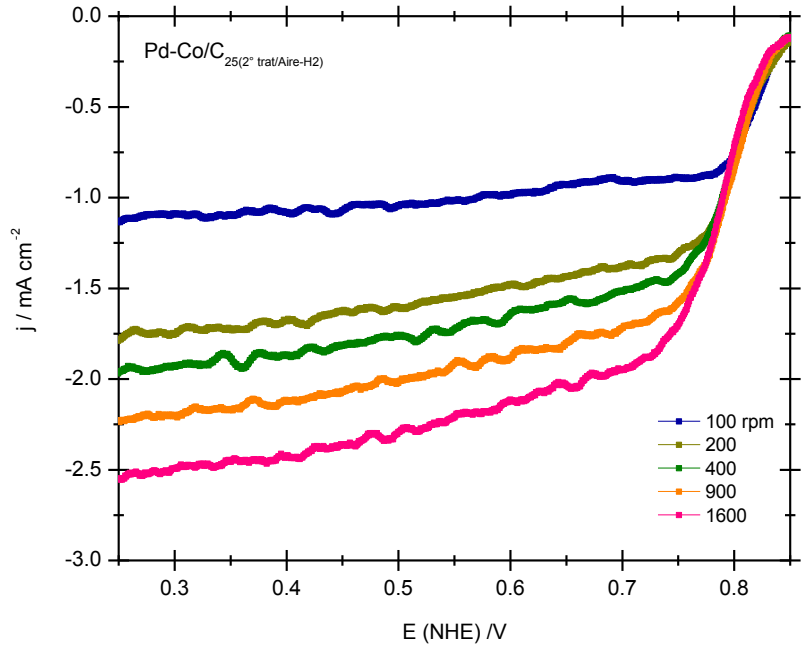

Figure 7. Steady-state polarization curves for the ORR on $(Pd\text{-}Co/C_{25})_3$ electrocatalyst in O_2-saturated 0.5 M H_2SO_4 electrolyte at 25°C.

As the particle size of the catalyst decreases, an enhancement of the current density is observed; this behavior is associated with the proton adsorption/desorption peaks of the hydrogen in the region from 0.0-0.3 V/NHE. On the cathodic site, OH_{ad} is favored onto the $(Pd\text{-}Co/C_{25})_3$

electrocatalyst, by the second metal and the thermal treatment of the bimetallic PdCo/C, which shifts the hydroxide reduction potential from approximately 0.03V to a more positive value in relation to the as synthesized Pd electrocatalysts. An increase in the cathodic current density at 0.6 V/NHE is associated with elevated concentrations of the anions previously adsorbed and reduced at this electrode potential, which indicates that the $(Pd\text{-}Co/C_{25})_3$ electrocatalyst poses a higher oxygen adsorption capacity than Pd alone.

However, due to the low solubility of oxygen in acidic media, the ORR depends strongly on the hydrodynamic conditions.

During the electrochemical reactions, the charge transfer and the mass transfer are two consecutive processes involved in the ORR and distinguished from polarization curves.. It is accepted that the first electron transfer on oxygen adsorption together with an electron and proton transfer forming superoxide is the rate-determining step on a Pt surface. In a bimetallic compound a more reactive surface with a higher d-band center tends to bond the oxygen molecule more strongly, and consequently, the electron transfer and O-O bond breaking, are more easier. The ORR characteristic RDE polarization curves for the nanometric $(Pd\text{-}Co/C_{25})_3$ electrocatalyst, at different rotation rates are shown in Figure 7. At the beginning of the scan potential, in the negative direction from the open circuit potential, -0.92 V/NHE at low overpotential, a defined charge transfer control is observed for which the current density is independent of the electrode rotation speed. The mixed kinetic-diffusion control region (-0.9 to -0.8 V/NHE) is followed by the appearance of a diffusion-limiting current region. As the rotation rate increases, the current also increases due to an enhancement of the oxygen diffusion through the thin-film electrode surface. Therefore, the overall measured current of the oxygen reduction can be considered to depend on the kinetic current density, j, the diffusion-limited current density, j_L, and the diffusional current density in the Nafion film, j_f. This diffusional current density can be considered insignificant when applied as a very thin film, which is the case in the present study and equation 1 can be applied, [24].

$$\frac{1}{j} = \frac{1}{j_k} + \frac{1}{j_L} + \frac{1}{j_f} = \frac{1}{j_k} + \frac{1}{B\omega^{1/2}} \qquad (1)$$

From the Koutecky-Levich plot (not included), a linear relationship between j^{-1} and □□□□□was obtained, indicating first order kinetics for the PdCo with respect to the oxygen reduction reaction within the potential range studied. The experimental average slope value, B_{exp} = 15.23 x10^{-2} mA cm^{-2} $rpm^{-1/2}$, was in agreement with the theoretical slope, B_{th}= 12.65 x 10^{-2} mA cm^{-2} $rpm^{-1/2}$, calculated for the four-electron transfer process leading to water formation. The kinetic current is proportional to the intrinsic properties of the catalyst; the catalytic activity of a material can be measured in terms of the parameters deduced from the mass transfer-corrected Tafel slope. Figure 8 shows the mass transfer-corrected Tafel plot for the nanometric Pd as synthesized and for the thermally treated PdCo in an oxygen-saturated 0.5 M H_2SO_4 solution deduced from Figure 7 and using equation 2.

$$j_k = \frac{j\, j_L}{j_L - j} \qquad (2)$$

The electrocatalytic response of the Tafel slope for each electrocatalyst shows a linear behavior at a high current density from which kinetic parameters were obtained. The kinetic parameters deduced from the analysis of the Tafel slope at a high overpotential are summarized in Table 2.

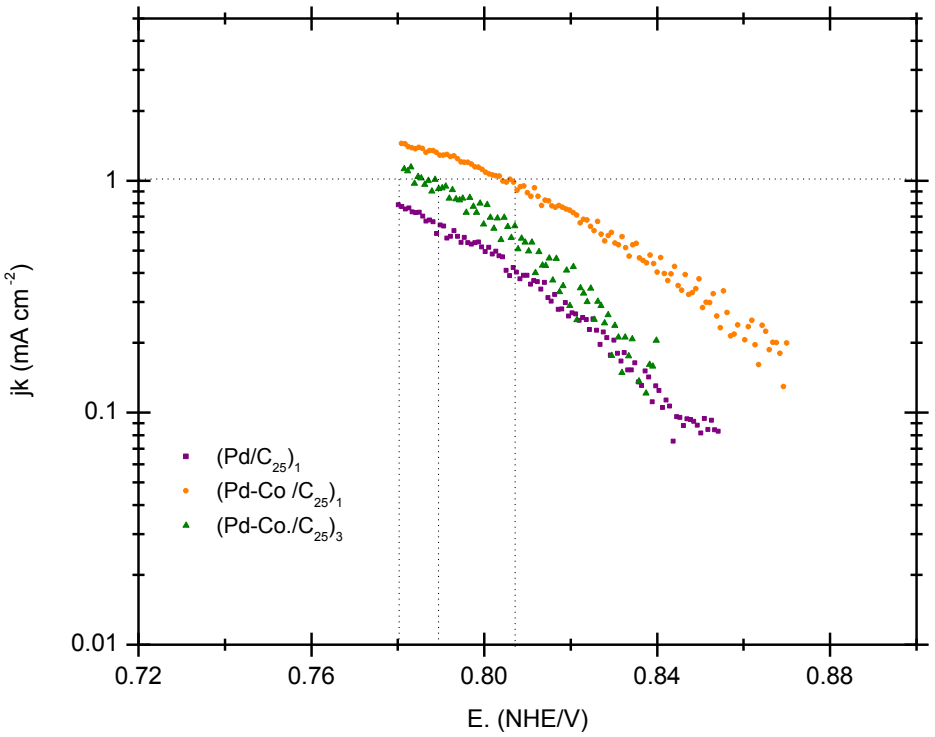

Figure 8. Mass-transfer corrected Tafel plots for the ORR on Pd-based electrocatalysts in O_2-saturated 0.5 M H_2SO_4 electrolyte at 25°C

It is well known that the rate of the cathodic reaction is proportional to the exchange current density, i_o, and exponentially related to the Tafel slope. It is desirable to minimize the Tafel slope in order to achieve a high voltage for the high operating current density. The deduced Tafel slope of the nanometric PdCo/C is similar to that reported in literature; this indicates that the bimetallic catalyst activity for the same ORR is attributed to the bi-functional effect in which the catalytic properties of each of the elements combine in a synergetic manner to yield a more active surface than Pd and Co alone.

Table 2. Kinetic parameters deduced from the Tafel slope for the ORR on Pd-based electrocatalysts in 0.5 M H_2SO_4 at 25°C.

Electrocatalysts	Tafel slope /mVdec^{-1}	Transfer coefficient	io/ mA cm^{-2}
(Pd/C25)1	70.2	0.84	3.011x10^{-7}
(Pd-Co/C25)1	93.6	0.63	2.89x10^{-5}
(Pd-Co/C25)3	96	0.61	3.02x10^{-5}

4. CONCLUSIONS

This article describes and discusses the activity of Pd and PdCo nanocatalysts for the oxygen reduction reaction in acid media. The preparation of monometallic Pd and bimetallic Pd-Co catalysts via the successive chemical reduction of metallic precursors allowed a successfully formation of nanometric particles with 5 to 15 nm sizes with spherical and defined surface structures, which was corroborated by both UV-Vis and TEM studies. The electrochemical characterization shows that synthesized materials are assets to the ORR. The deduced kinetic parameters indicate that the bimetallic catalyst exhibits a better catalytic activity for the ORR, attributed to the bi-functional effect in which the catalytic properties of each of the elements combine in a synergetic manner to yield a more active surface than Pd alone.

ACKNOWLEDGMENTS
We gratefully acknowledge the support of Mexico's National Council of Science and Technology, CONACYT, under grant 101357. AVM thanks CONACYT for the Master of science fellowship.

References

1. Purwanto, W.W., Wargadalam, V.J., Pranoto, B., *Int. J. Electrochem. Sci.* 7 (2012) 525-533.
2. Naohara, H., Okamoto, Y., Toshima, N., J. Power Sources 196 (2011)7510-7513.
3. Stamenkovic, V.R., Simon, B., Arenz, M., Mayrhofer, K.J., Lucas, C.A., Wang, G., Ross, P.N., Markovic, N.M., *Nature Materials* 6 (2007) 241-247.
4. Burbe, L.D., Casey, J.K., *J. Electrochem. Soc.* 140 (1993) 1284-1291.
5. Mustain, W.E., Prakash, J., *J. Powers Sources 170* (2007) 28-37.
6. Shao, M.H., Huang, T., Liu, P., Zhang, J., Sasaki, K., Vukmirovic, M.B., Adzic, R.R., *Langmuir 22* (2006) 10409-10415.
7. Wang, Y.X., Balbuena, P.B., *J. Phys. Chem. B* 109 (2005) 18902.
8. Mustain, W.E., Kepler, K., Prakash, J., *Electrochem. Comer. 8* (2006) 406-410.
9. Zhang, L., Lee, K., Zhang, J., *Electrochem. Acta 52* (2007) 3088-3094.
10. Zhang, L., Lee, K., Zhang, J., *Electrochim. Acta* 52 (2007) 7964-7971.
11. Ramos-Sánchez, G., Bruno, M.M., Thomas, Y.R., Corti, H. R., Solorza-Feria, O., *Int. J. Hydrogen Energy* 37 (2012) 31-40.
12. Savadogo, O., Lee, K., Oishi, K., Mitsushima, S., Kamiya, N., Ota, K.I., *Electrochem. Comm. 6* (2004) 105-109.
13. Fouda-Onana, F., Bah, S., Savadogo, O., *J. Electroanal. Chem.* 636 (2008) 1-9.
14. Kim, J., Momma, T., Osaka, T., *Journal of Power Sources* 189 (2009) 909-915.
15. Fernández, J.L., Walsh, D.A., Bard, A.J., *J. Am. Chem. Soc.* 127 (2005) 357.
16. Wang, W., Zheng, D., Dua, C., Zoua, Z., Zhang, X., Xia, B., Yang, H., Akins, D., *J. of Power Sources* 167 (2007) 243-249.
17. Li, X., Huang, Q., Zou, Z., Xia, B., Yang, H., *Electrochem. Acta* 53 (2008) 6662-6667.
18. Teranishi, T., Miyake, M., *Chem. Mater.* 10 (1998) 594-600.
19. Peng, H., Yong, K., Liu, H., *J. Mater. Chem.* 12 (2002) 934-937.
20. Ruíz Camacho B., *"Síntesis, caracterización y evaluación de nanoparticulas de Pi y Pt-Au para su aplicación en una celda de combustible a base de hidrógeno (PEM),* UAM-Azcapotzalco, México, 2007.
21. Busser, G.W., Van Ommen, J.G., Lercher, J.A., *J. Phys. Chem.* B 103 (1999) 1651-1659.

22. Toshima, N., Yonezawa, T., New *J. Chem.* 22 (1998) 1179-1201.
23. Nemamacha, A., Rehspringer, J.L., Khatmi, D., *J. Phys. Chem. B 110* (2006) 383-387.
24. K. Sasaki, J. X. Wang, H. Naohara, N. Marinkovic, K. More, H. Inada, and R. R. Adzic, *Electrochim. Acta*, **55**, 2645 (2010).
25. Bard AJ, Faulkner L. Electrochemical methods: fundamentals and applications. New York: Wiley; 2001. p. 341.